Formation and Properties of Stabilized Aluminum Nanoparticles

Mohammed J. Meziani,[†] Christopher E. Bunker,*[,‡] Fushen Lu,[†] Heting Li,[†] Wei Wang,[†] Elena A. Guliants,[§] Robert A. Quinn,[†] and Ya-Ping Sun*[,†]

Department of Chemistry and Laboratory for Emerging Materials and Technology, Clemson University, Clemson, South Carolina 29634-0973, Air Force Research Laboratory, Propulsion Directorate, Wright-Patterson Air Force Base, Ohio 45433-7103, and Sensors Technology Office, University of Dayton Research Institute, Dayton, Ohio 45469

ABSTRACT The wet-chemical synthesis of aluminum nanoparticles was investigated systematically by using dimethylethylamine alane and 1-methylpyrrolidine alane as precursors and molecules with one or a pair of carboxylic acid groups as surface passivation agents. Dimethylethylamine alane was more reactive, capable of yielding well-defined and dispersed aluminum nanoparticles. 1-Methylpyrrolidine alane was less reactive and more complex in the catalytic decomposition reaction, for which various experimental parameters and conditions were used and evaluated. The results suggested that the passivation agent played dual roles of trapping aluminum particles to keep them nanoscale during the alane decomposition and protecting the aluminum nanoparticles postproduction from surface oxidation and that an appropriate balance between the rate of alane decomposition (depending more sensitively on the reaction temperature) and the timing in the introduction of the passivation agent into the reaction mixture was critical to the desired product mixes and/or morphologies. Some fundamental and technical issues on the alane decomposition and the protection of the resulting aluminum nanoparticles are discussed.

KEYWORDS: aluminum nanoparticles • alanes • surface passivation • energetic nanomaterials

INTRODUCTION

There has been significant recent interest in the synthesis and properties of nanoscale reactive metal particles, especially aluminum nanoparticles, for a number of current and potential applications (1−9). The large specific surface area and energy density and their associated high reactivity of aluminum nanoparticles have made them unique combustible additives in propellant formulations for significantly higher and faster energy release.

Nanoscale aluminum may also offer significant opportunities in the development of high-capacity hydrogen storage materials, either directly or through other reactive compounds such as aluminum hydrides. Recently, reactive aluminum compounds were nanosized for improving their hydrogen-storage-related properties (10−12). These nanoparticles supported on surface-oxidized carbon nanofibers or confined in ordered mesoporous silica exhibited lower dehydrogenation temperature and faster kinetics than those of their corresponding bulk materials (10−12).

Much effort has been devoted to the synthesis of small aluminum nanoparticles that are stabilized by coatings or organic surface passivation agents for protection from rapid oxidation to aluminum oxide under ambient conditions (13−22). Such surface oxidation could have aluminum oxide accounting for 60% or more of the mass in a particle of 50 nm or less in diameter. In the preparation by physical methods, including mechanical attrition (high-energy ball milling) and vapor condensation (21, 22), the resulting aluminum nanoparticles are first collected and then surface-passivated via slow oxidation or by use of various organic substances (13−16, 21, 22). However, these physical nanosizing schemes are often limited for their generally producing particles of rather broad size distributions, such as particle diameters from 50 nm to more than 1 μm.

The wet-chemical synthesis of aluminum nanoparticles has been explored by using alanes as precursors in thermal and/or catalytic decomposition reactions (17−20). For example, Foley and co-workers synthesized aluminum nanoparticles through alane thermal decomposition in solution (19). The nanoparticles were coated with another metal (gold, nickel, palladium, or silver) for protection from oxidation, for which the nickel coating was found to be more effective (19). These metal-coated aluminum nanoparticles were on the order of 150 nm in size. Separately, Jouet and co-workers found that organic molecules such as perfluorinated carboxylic acids could be included in the alane decomposition reactions for their effective passivation of the formed aluminum nanoparticles (20). The results from all of the investigations already reported in the literature suggest great potential of the wet-chemical approach in not only the particle passivation but also the manipulation and eventually the control of other particle properties such as the average

* Corresponding authors. E-mail: Christopher.Bunker@WPAFB.AF.MIL (C.E.B.), syaping@clemson.edu (Y.-P.S.). Fax: 937-255-5525 (C.E.B.), 864-656-5007 (Y.-P.S.).

Received for review December 5, 2008 and accepted February 4, 2009

[†] Clemson University.

[‡] Wright-Patterson Air Force Base.

[§] University of Dayton Research Institute.

DOI: 10.1021/am800209m

size, size distribution, morphology, and homogeneous dispersion of the nanoparticles in solution.

We report here a more systematic investigation on the wet-chemical synthesis of aluminum nanoparticles from different alanes under various experimental conditions and with the use of molecules containing mono- or difunctional groups for the particle surface passivation. Some fundamental and technical issues on the alane decomposition and the protection of the resulting aluminum nanoparticles are discussed.

EXPERIMENTAL SECTION

Materials. The dimethylethylamine alane, $H_3AlN[(CH_3)_2C_2H_5]$, in a toluene solution was supplied by Sigma-Aldrich and so were titanium(IV) isopropoxide, lithium aluminum hydride ($LiAlH_4$), anhydrous aluminum chloride, perfluorotetradecanoic acid ($C_{13}F_{27}COOH$), 1*H*,1*H*-perfluoro-1-tetradecanol ($C_{13}F_{27}CH_2OH$), tetradecanoic acid, dimethyl-5-hydroxybenzene-1,3-dicarboxylate, octadecylamine, and 1-methylpyrrolidine. The solvents diethyl ether, tetrahydrofuran (THF), hexane, and toluene were distilled over sodium metal before use. Other solvents either were spectrophotometry/HPLC-grade or were purified via simple distillation. Deuterated NMR solvents were obtained from Cambridge Isotope Laboratories.

The 1-methylpyrrolidine alane, $H_3AlN[(C_4H_8)(CH_3)]$, was prepared according to procedures already reported in the literature (23, 24). Briefly, in a glovebox, *N*-methylpyrrolidine (13.6 g, 16.6 mL) was added dropwise to a suspension of aluminum chloride (2.64 g, 20 mmol) and $LiAlH_4$ (2.58 g, 68 mmol) in hexane (30 mL) at room temperature (22 °C) with vigorous stirring. The reaction mixture was further stirred for about 12 h more, filtered, and rinsed twice with hexane (15 mL each). The filtrate was collected and evaporated under vacuum for removal of all volatile components to yield $H_3AlN[(C_4H_8)(CH_3)]$.

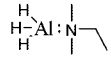

$H_3AlN[(CH_3)_2C_2H_5]$

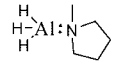

$H_3AlN[(C_4H_8)(CH_3)]$

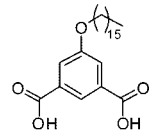

HDIPA

5-(Hexadecyloxy)isophthalic acid (HDIPA) was also prepared by following procedures available in the literature (25). Briefly, dimethyl-5-hydroxyisophthalate (7.5 g, 36 mmol) and potassium carbonate (9.8 g, 71 mmol) were mixed and stirred in *N*,*N*-dimethylformamide (DMF; 200 mL) at 80 °C for 1 h. A solution of 1-bromohexadecane (13.1 g, 43 mmol) in DMF (25 mL) was added dropwise, and the mixture was stirred for another 6 h. The reaction mixture was concentrated and poured into water, from which dimethyl-5-(hexadecyloxy)isophthalate was extracted with dichloromethane. The sample was recrystallized, followed by base-catalyzed hydrolysis into HDIPA. ^{1}H NMR (500 MHz, DMSO-d_6): δ 13.28 (s, 2H), 8.04 (s, 1H), 7.61 (s, 2H), 4.04 (t, 2H), 1.68−1.72 (m, 2H), 1.38−1.41 (m, 2H), 1.20−1.32 (m, 24H), 0.83 (t, 3H). ^{13}C NMR (125.7 MHz, DMSO-d_6): δ 166.86, 159.20, 133.03, 122.61, 119.36, 68.44, 31.80, 29.57, 29.51, 29.28, 29.24, 29.04, 25.90, 22.58, 14.30.

Measurements. Air- and moisture-sensitive materials were handled in an argon-filled glovebox. NMR spectra were obtained on a JEOL Eclipse +500 NMR spectrometer or a Bruker Advance 500 NMR spectrometer. Thermogravimetric analysis (TGA) was carried out on a Mettler-Toledo TGA/SDTA851e or a TA Q500 system. Powder X-ray diffraction (XRD) measurements were performed on a Scintag XDS-2000 powder diffraction system. Electron microscopy imaging was conducted on a Hitachi HD-2000 scanning transmission microscopy (S-TEM) system in the SEM and Z-contrast modes. The specimen for the imaging was prepared by depositing a few drops of a dilute nanoparticle suspension onto a carbon-coated copper grid, followed by solvent evaporation under ambient conditions. The energy-dispersive X-ray (EDX) analysis was performed in situ on the same S-TEM system.

Reactions at Room Temperature. For $H_3AlN[(CH_3)_2C_2H_5]$, a toluene solution of the alane (0.5 M, 6.5 mL) was mixed with predegassed (bubbled nitrogen gas for 30 min) diethyl ether (10 mL) and stirred at room temperature (22 °C) in the argon-filled glovebox. To the solution was added titanium(IV) isopropoxide (8 μL) rapidly via a syringe. Upon stirring of the mixture 8 min, a solution of $C_{13}F_{27}COOH$ in diethyl ether (26 mM, 25 mL) was added, and the resulting mixture was stirred continuously for 12 h. At completion, the reaction mixture was allowed to settle, and the ether layer was removed. The brown-colored sediment was washed twice with diethyl ether, followed by the removal of residual ether via evaporation (all in the glovebox).

Similarly, $H_3AlN[(C_4H_8)(CH_3)]$ (284 mg, 2.47 mmol) was dissolved in predegassed diethyl ether (15 mL) and stirred in the glovebox. To the solution was added titanium(IV) isopropoxide (5 μL) rapidly via a syringe. The mixture was stirred for 8 min, 30 min, 60 min, 2 h, or 4 h before the addition of the $C_{13}F_{27}COOH$ solution in diethyl ether (32 mM, 15 mL), followed by stirring for another 12 h. Each mixture was allowed to settle before removal of the diethyl ether layer. The remaining sediment was washed twice with diethyl ether and then evaporated to remove the residual solvent (all in the glovebox).

The same procedures above were used for 1*H*,1*H*-perfluoro-1-tetradecanol ($C_{13}F_{27}CH_2OH$) or tetradecanoic acid ($C_{13}H_{27}COOH$) in place of $C_{13}F_{27}COOH$ as the surface passivation agent, with the same alane-to-passivation agent ratios and under otherwise the same experimental conditions. For use of HDIPA as the surface passivation agent, $H_3AlN[(C_4H_8)(CH_3)]$ (284 mg, 2.47 mmol) was dissolved in predegassed THF (15 mL) and stirred at room temperature in the glovebox. To the solution was added titanium(IV) isopropoxide (5 μL) rapidly via a syringe. The mixture was stirred for 8 min, 30 min, 2 h, or 4 h before the HDIPA solution in THF (32 mM, 15 mL) was added, followed by stirring for another 12 h. The reaction mixture was allowed to settle, and the THF layer was discarded. The remaining sediment was washed twice with THF and then evaporated for complete removal of residual THF (all in the glovebox).

Reactions at High Temperature. A solution of $H_3AlN[(C_4H_8)(CH_3)]$ (284 mg, 2.47 mmol) in predegassed toluene (15 mL) was prepared and heated to 110 °C under nitrogen in the glovebox. The solution was vigorously stirred while titanium(IV) isopropoxide (5 μL) was added quickly via a syringe, followed immediately or after up to a 30 min delay by the addition of the $C_{13}F_{27}COOH$ solution in a toluene/diethyl ether mixture (32 mM, 15 mL). The reaction mixture was further stirred for 30 min without heating. After the reaction, the mixture was centrifuged to discard the supernatant. The sediment was washed twice with diethyl ether and then evaporated to remove any residual ether (all in the glovebox).

For use of octadecylamine as the copassivation agent with $C_{13}F_{27}COOH$, octadecylamine (666 mg, 2.47 mmol) in predegassed toluene (10 mL) was prepared and heated to 90 °C under nitrogen in the glovebox. To the hot solution under vigorous stirring was added sequentially titanium(IV) isopropoxide (5 μL), the $H_3AlN[(C_4H_8)(CH_3)]$ solution in predegassed toluene (1.24 M, 2 mL), and then the $C_{13}F_{27}COOH$ solution in a toluene/diethyl ether mixture (0.1 M, 5 mL). After the reaction, the mixture was centrifuged to discard the supernatant. The sediment was washed twice with diethyl ether, followed by the removal of residual ether via evaporation (all in the glovebox).

N,*N*-Dimethylaniline (DMA; 10 mL) as the solvent was degassed and then heated to 90 °C under nitrogen in the glovebox.

Scheme 1. Catalytic Decomposition Reactions of Alanes

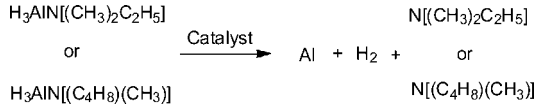

To the hot solvent with vigorous stirring was added the $H_3AlN[(C_4H_8)(CH_3)]$ solution in predegassed toluene (0.73 M, 2 mL) and titanium(IV) isopropoxide (5 μL). Subsequently, the $C_{13}F_{27}COOH$ solution in diethyl ether (60 mM, 5 mL) was added. After the reaction, the mixture was centrifuged to discard the supernatant. The sediment was washed twice with diethyl ether, followed by the removal of residual ether via evaporation (all in the glovebox).

Aluminum Tests. The contents of active aluminum in the samples of surface-passivated aluminum nanoparticles was determined in terms of the base hydrolysis method and/or by using TGA measurements. In the base hydrolysis (26), the active aluminum reduced water under basic conditions into hydrogen gas, whose quantity was determined volumetrically to calculate the amount of active aluminum. In TGA, the sample was scanned to 1000 °C in the presence of air, so that the weight gain due to the formation of aluminum oxide was used to calculate the original active aluminum content. The two tests were found to be consistent according to results from the calibration with samples of pure aluminum.

RESULTS AND DISCUSSION

The two alane compounds $H_3AlN[(CH_3)_2C_2H_5]$ and $H_3AlN[(C_4H_8)(CH_3)]$ could both be decomposed with organotitanium(IV) as a catalyst (Scheme 1) (18, 20). However, the formation of aluminum nanoparticles from decomposition was quite different between the different alanes and also significantly dependent on other experimental parameters.

The alane $H_3AlN[(CH_3)_2C_2H_5]$ was obviously more readily decomposed than the other alane $H_3AlN[(C_4H_8)(CH_3)]$ at room temperature. For the former, the catalytic decomposition was already substantial after reaction at room temperature for only a short period of time (8 min or so), when the surface passivation agent $C_{13}F_{27}COOH$ was added to help trap the nanoscale aluminum, resulting in the formation of well-defined aluminum nanoparticles. According to S-TEM imaging results (Figure 1), these surface-passivated nanoparticles were averaging 48 nm in diameter, with a size distribution standard deviation of 15 nm. The EDX analysis of the specimen confirmed the presence of high relative concentrations of aluminum and fluorine (in the passivation agent $C_{13}F_{27}COOH$) but only a small amount of oxygen, consistent with the expectation for the surface-protected aluminum nanoparticles without any significant oxidation. The XRD pattern of the nanoparticle sample exhibited no obvious peaks, suggesting that the aluminum nanoparticles were largely amorphous. This was consistent with the results from high-resolution TEM imaging of the nanoparticles showing no obvious crystalline fringes. The Fourier transform infrared (FT-IR) spectrum of the passivation agent capping the aluminum nanoparticles differed from that of free molecules in terms of diminished carbonyl absorption around 1750 cm^{-1} (Figure 2), in agreement with similar observations already reported in the literature (20).

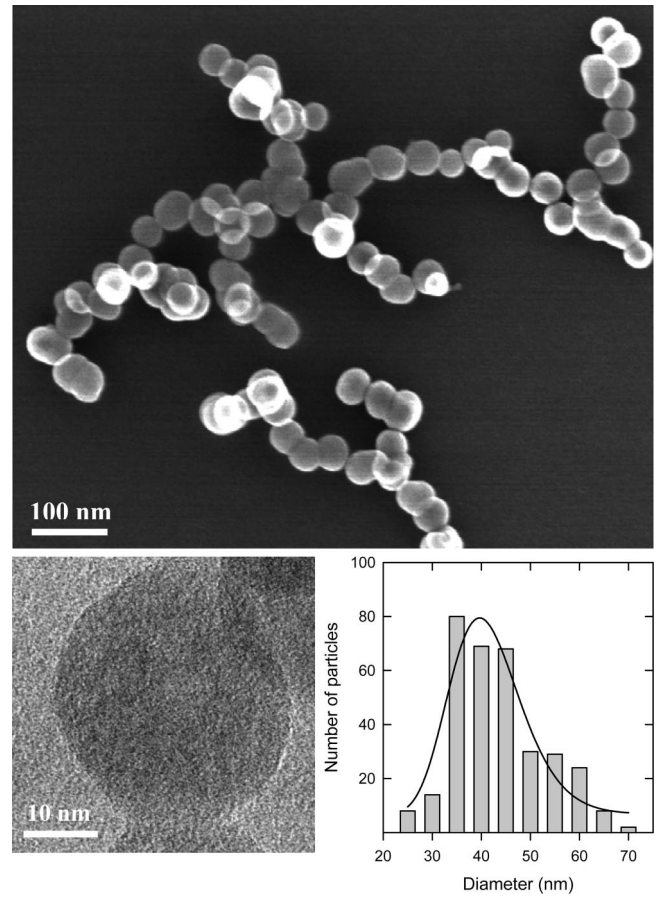

FIGURE 1. S-TEM (SEM mode) image (top) and high-resolution TEM image (bottom left) of the aluminum nanoparticles from $H_3AlN[(CH_3)_2C_2H_5]$ (some of the passivation agent removed in the preparation of specimen for imaging) and a statistical analysis based on multiple SEM images (bottom right).

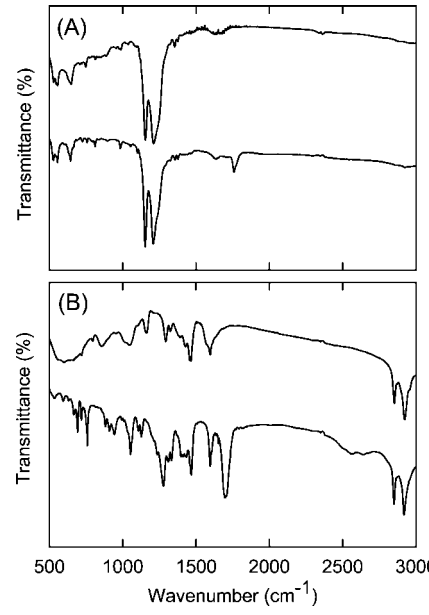

FIGURE 2. FT-IR spectra of (A) $C_{13}F_{27}COOH$ capping the aluminum nanoparticles (upper) versus free (lower) and (B) HDIPA capping the nanoparticles (upper) versus free (lower).

The relatively rapid decomposition of the alane $H_3AlN[(CH_3)_2C_2H_5]$ probably enabled kinetically controlled processes for the formation and trapping of more homoge-

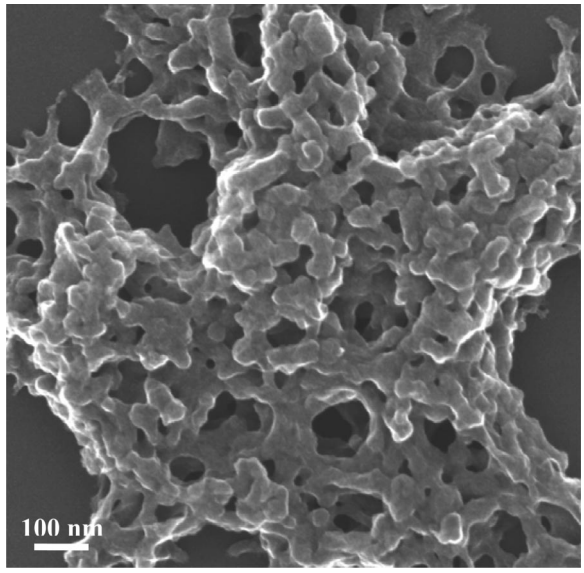

FIGURE 3. Representative S-TEM (SEM mode) image on aluminum nanoparticle samples from some repeats of the $H_3AlN[(CH_3)_2C_2H_5]$ decomposition reaction with $C_{13}F_{27}COOH$ as the passivation agent.

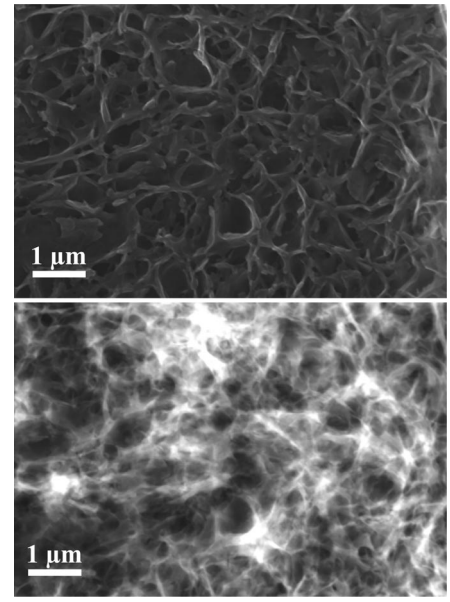

FIGURE 4. S-TEM images (top, SEM mode; bottom, Z-contrast mode) on a sample from $H_3AlN[(CH_3)_2C_2H_5]$ decomposition with a much higher passivation agent $C_{13}F_{27}COOH$ concentration.

neously distributed aluminum nanoparticles (Figure 1). However, the same high reactivity could also be problematic in terms of the reaction reproducibility and control. The catalytic decomposition resulting in the well-defined aluminum nanoparticles could only be achieved by using a fresh alane sample, and even with the use of only freshly acquired alane samples, there were significant batch-to-batch variations. Many such experiments designed specifically for exact repeats resulted in more complex product mixtures of a composite-like morphology (Figure 3), which might be attributed to the reaction being relatively sensitive to the precursor alane sample and perhaps also to some subtle differences in the experimental conditions. A somewhat different morphology of composites based on fiberlike structures could also be observed by doubling the amount of the passivation agent used in the reaction while keeping the alane and all other experimental parameters the same (Figure 4).

The alane $H_3AlN[(CH_3)_2C_2H_5]$ is also relatively expensive, which may limit its use as a precursor in the scale-up production of aluminum nanoparticles. In this regard, the alane $H_3AlN[(C_4H_8)(CH_3)]$ could offer some advantages. It was explored as a precursor for aluminum nanoparticles more systematically in this study.

The catalytic decomposition of the alane $H_3AlN[(C_4H_8)(CH_3)]$ was obviously less efficient under the same experimental conditions as those described above for $H_3AlN[(CH_3)_2C_2H_5]$, generally yielding more complex product mixtures that contained only minor aluminum particles according to results from electron microscopy analyses and the classical volumetric base-hydrolysis test (measuring the active aluminum content in the sample in terms of the volume of hydrogen gas produced) (26). The poorer yields of aluminum nanoparticles from $H_3AlN[(C_4H_8)(CH_3)]$ could be attributed to this alane being relatively more stable, requiring more time for the decomposition reaction before the addition of the surface passivation agent.

The reaction time allowed for the catalytic decomposition of $H_3AlN[(C_4H_8)(CH_3)]$ in the absence of the passivation agent was apparently critical to the composition and morphology of the product mixture. For example, at the same alane-to-passivation agent molar ratio of 5:1, when the reaction time for $H_3AlN[(C_4H_8)(CH_3)]$ decomposition (Scheme 1) at room temperature was increased from 8 min to 2 h before the passivation agent $C_{13}F_{27}COOH$ was added to the reaction mixture, the resulting product mixture contained many more aluminum particles. According to the results from the base-hydrolysis test and TGA measurements, the conversion from alane to aluminum was more than 90% under the conditions of the reaction for 2 h before the addition of the passivation agent. The product mixtures thus obtained were prepared into specimens for electron microscopy analyses, from which the results consistently exhibited relatively larger (100−200 nm) aluminum nanoparticles mixed with the passivation agent in a composite-like morphology (similar to what is shown in Figure 3). The EDX analyses of the same specimens suggested the presence of high aluminum and fluorine contents and very low oxygen, again as expected for the $C_{13}F_{27}COOH$-protected aluminum nanoparticles without any significant contamination by aluminum oxide. The aluminum nanoparticles in these samples were more crystalline according to powder XRD results. In the diffraction pattern, the aluminum peak was broadened (Figure 5), from which the width was used with the Scherrer equation (27) to estimate the average size of the aluminum particles. The particle diameter thus calculated was about 150 nm, in reasonable agreement with the observation in electron microscopy analyses.

The passivation agent apparently played dual roles of keeping the aluminum particles nanoscale in their formation and also protecting the formed nanoparticles from oxidation.

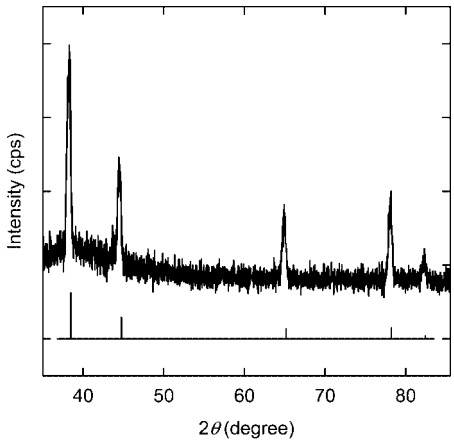

FIGURE 5. XRD pattern of the $C_{13}F_{27}COOH$-passivated aluminum nanoparticles (average size ~ 150 nm), with the standard pattern of aluminum from the XRD database for comparison.

Thus, several passivation molecules of different structures and functionalities were compared and evaluated with the use of $H_3AlN[(C_4H_8)(CH_3)]$ as a precursor for aluminum nanoparticles. The fluorinated alcohol $C_{13}F_{27}CH_2OH$ is both structurally and functionally somewhat similar to $C_{13}F_{27}COOH$ because the proton in fluorinated alcohol is known to be highly acidic. In general, however, the alcohol was a much less effective passivation agent than the corresponding acid under otherwise the same experimental conditions. The addition of the alcohol to the reaction mixture (even after only a short delay such as 8 or 30 min) did not trap nanoscale aluminum particles, and instead the particles kept growing into larger sizes (beyond 200 nm). On the other hand, the nonfluorinated acid $C_{13}H_{27}COOH$ was similar to its perfluorinated counterpart as the passivation agent in the catalytic decomposition reaction of $H_3AlN[(C_4H_8)(CH_3)]$ under various experimental conditions.

The effectiveness of the passivation agent with a pair of carboxylic acids, HDIPA, was evaluated. For the function of trapping aluminum particles to keep them nanoscale, HDIPA was similar to both $C_{13}H_{27}COOH$ and $C_{13}F_{27}COOH$. In the reaction, HDIPA also interfered with the decomposition of $H_3AlN[(C_4H_8)(CH_3)]$, with a reaction time of close to 2 h required without HDIPA in the reaction mixture for a complete alane-to-aluminum conversion. Further prolonging the reaction time beyond 2 h (before the addition of HDIPA) resulted in larger and crystalline aluminum particles of various shapes (Figure 6). These HDIPA-protected aluminum nanocrystals were highly stable in ambient air, without the surface being oxidized over at least days (the same TGA traces obtained for the sample over the time period). The FT-IR spectrum of the HDIPA capping the aluminum nanoparticles again exhibited diminished carbonyl absorption around 1710 cm^{-1} (Figure 2) due to significant carboxylate–aluminum surface interactions.

The results described above on the alane $H_3AlN[(C_4H_8)(CH_3)]$ obviously suggest that a more efficient catalytic decomposition to allow the prompt addition of the selected passivation agent would be favorable to both the desired complete alane-to-aluminum conversion and the formation of smaller aluminum nanoparticles. At room temperature,

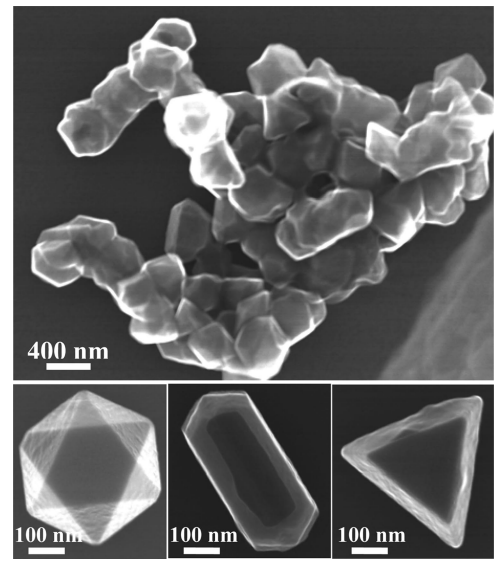

FIGURE 6. S-TEM (SEM mode) images on a sample from $H_3AlN[(C_4H_8)(CH_3)]$ decomposition at room temperature for 4 h before the addition of the passivation agent HDIPA.

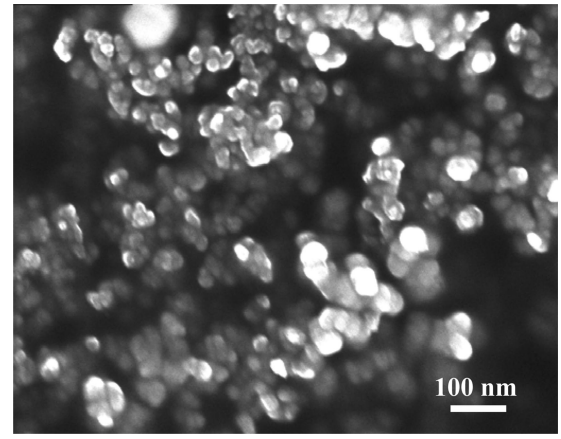

FIGURE 7. Field-emission SEM image on aluminum nanoparticles from the $H_3AlN[(C_4H_8)(CH_3)]$ reaction in hot toluene (110 °C) for 20 min before the addition of the passivation agent $C_{13}F_{27}COOH$.

the use of much higher catalyst concentration (3 times, for example) hardly improved the decomposition efficiency and the overall results of aluminum nanoparticles. More effective were higher reaction temperatures with otherwise similar experimental parameters or under different experimental conditions. For example, the catalytic decomposition reaction of $H_3AlN[(C_4H_8)(CH_3)]$ in hot toluene (110 °C) was much more efficient. When the reaction was allowed to proceed for 20 min before the addition of the passivationa agent $C_{13}F_{27}COOH$, the alane-to-aluminum conversion was essentially quantitative. According to results from electron microscopy analyses, the product mixture contained mostly aluminum nanoparticles of 50–100 nm size (Figure 7).

In an effort to improve the distribution and dispersion of aluminum nanoparticles, octadecylamine (a molecule commonly used in the nanoparticle synthesis) was used as a copassivation agent with $C_{13}F_{27}COOH$. Experimentally, the reaction conditions were generally similar to those described above, except for some changes in the sequence of the addition of various reagents. The resulting aluminum nano-

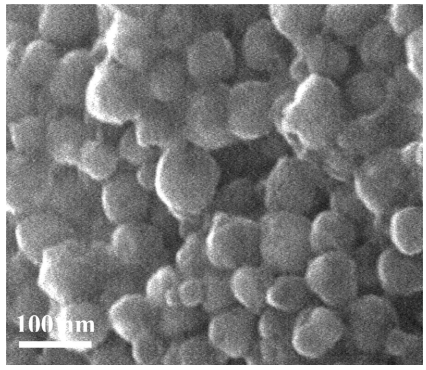

FIGURE 8. Representative S-TEM (SEM mode) image on aluminum nanoparticles from the $H_3AlN[(C_4H_8)(CH_3)]$ reaction in hot toluene with octadecylamine as a copassivation agent with $C_{13}F_{27}COOH$.

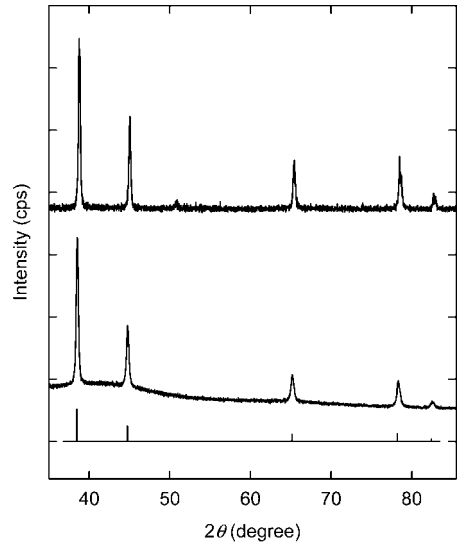

FIGURE 9. XRD patterns of the surface-passivated aluminum nanoparticles synthesized in hot toluene with octadecylamine (upper) and in hot DMA (lower), with the standard pattern of aluminum from the XRD database for comparison.

particles protected by a combination of $C_{13}F_{27}COOH$ and octadecylamine appeared better in dispersion according to electron microscopy imaging results (Figure 8). A statistical analysis of the microscopy images yielded an average particle size of 75 nm in diameter and a size distribution standard deviation of 19 nm. Here the role of octadecylamine, in addition to it being a commonly used surface passivation agent for inorganic nanoparticles, might also include acid−base interactions with $C_{13}F_{27}COOH$ to enhance its intended function. The XRD pattern of the sample is shown in Figure 9, confirming the presence of nanoscale aluminum. In terms of the same logic, DMA was used to replace toluene as the reaction solvent at a high reaction temperature (90 °C), but only $C_{13}F_{27}COOH$ was used as the passivation agent. The catalytic decomposition of $H_3AlN[(C_4H_8)(CH_3)]$ under the experimental conditions was efficient, yielding relatively smaller aluminum nanoparticles (mostly less than 50 nm) according to electron microscopy imaging results (Figure 10). The XRD pattern of the aluminum nanoparticles is also shown in Figure 9 for comparison.

The strong affinity of carboxylic acid groups to the aluminum metal surface has been well-documented in the

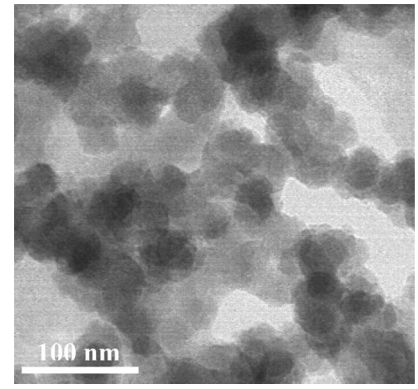

FIGURE 10. TEM image on aluminum nanoparticles from the $H_3AlN[(C_4H_8)(CH_3)]$ reaction in hot DMA.

literature based on both experimental and theoretical studies (28−32). For example, the strong interactions between carboxylate species and aluminum atoms and the corresponding structural configurations were demonstrated in the study of aluminum atoms deposited onto a carboxy-terminated self-assembled monolayer on a gold substrate (30). The requirement for two oxygen heads in a carboxylate group to achieve the surface passivation of aluminum nanoparticles was demonstrated by the obviously poor performance of the fluorinated alcohol. As mentioned earlier, HDIPA with a pair of carboxylic acids (thus two pairs of oxygen heads) was effective in the protection of formed aluminum nanoparticles from surface oxidation. $C_{13}F_{27}COOH$ was also effective, probably at least in part because of its very high acidity (thus closer to the carboxylate). Its nonfluorinated counterpart $C_{13}H_{27}COOH$ appeared to be somewhat less effective in the protection of aluminum nanoparticles from surface oxidation, though a more quantitative comparison based on more accurate evaluation methods is still required.

In summary, both alanes $H_3AlN[(CH_3)_2C_2H_5]$ and $H_3AlN[(C_4H_8)(CH_3)]$ could be catalytically decomposed, with the aid of a passivation agent, into aluminum nanoparticles. The former is more reactive, capable of yielding well-defined nanoparticles, while the latter is more complex in decomposition, so that manipulations of the experimental parameters and conditions are necessary. The passivation agent plays dual roles of trapping aluminum particles to keep them nanoscale during the alane decomposition and also protecting the aluminum nanoparticles postproduction from surface oxidation. As a result, an appropriate balance between the rate of alane decomposition (depending more sensitively to the reaction temperature) and the timing in the introduction of the passivation agent into the reaction mixture is critical to the desired product mixes and/or morphologies. The use of a passivation agent with a pair of functional groups responsible for interactions with the aluminum surface is beneficial at least to the postproduction protection of the aluminum nanoparticles. Further studies of the alane decomposition reaction under other conditions, including, for example, those with extremely rapid mixing and/or the use of a passivation agent mixture, should be valuable to the

more predictable or controllable production of well-dispersed stable aluminum nanoparticles.

Acknowledgment. Financial support from the Air Force Research Laboratory through the nanoenergetics program is gratefully acknowledged. Additional support from the South Carolina Space Grant Consortium (Y.-P.S.), the Air Force Office of Scientific Research (AFOSR) through the program of Dr. Julian Tishkoff (C.E.B.), and the Defense Threat Reduction Agency (DTRA) through Grant HDTRA-07-1-0026 (E.A.G.) is also acknowledged. R.A.Q. was an undergraduate research assistant supported by the Center for Advanced Engineering Fibers and Films (CAEFF, an NSF-ERC at Clemson University).

REFERENCES AND NOTES

(1) Ivanov, G. V.; Tepper, F. *4th Int. Symp. Spec. Top. Chem. Propul.* **1997**, 636.
(2) Mench, M. M.; Kuo, K. K.; Yeh, C. L.; Lu, Y. C. *Combust. Sci. Technol.* **1998**, *135*, 269–292.
(3) Brousseau, P.; Anderson, C. J. *Propellants, Explos., Pyrotech.* **2002**, *27*, 300–306.
(4) Jones, D. E. G.; Turcotte, R.; Fouchard, R. C.; Kwok, Q. S. M.; Turcotte, A. M.; Abdel-Qader, Z. *Propellants, Explos., Pyrotech.* **2003**, *28*, 120–131.
(5) Ivanov, Y. F.; Osmonoliev, M. N.; Sedoi, V. S.; Arkhipov, V. A.; Bondarchuk, S. S.; Vorozhtsov, A. B.; Korotkikh, A. G.; Kuznetsov, V. T. *Propellants, Explos., Pyrotech.* **2003**, *28*, 319–333.
(6) Granier, J. J.; Pantoya, M. L. *Combust. Flame* **2004**, *138*, 373–383.
(7) Eisenreich, N.; Fietzek, H.; Juez-Lorenzo, M. D.; Kolarik, V.; Koleczko, A.; Weiser, V. *Propellants, Explos., Pyrotech.* **2004**, *29*, 137–145.
(8) Teipel, U. *Energetic Materials*; Wiley-VCH: Weinheim, Germany, 2004.
(9) Gromov, A.; Ilyin, A.; Forter-Barth, U.; Teipel, U. *Propellants, Explos., Pyrotech.* **2006**, *31*, 401–409.
(10) Balde, C. P.; Hereijgers, B. P. C.; Bitter, J. H.; de Jong, K. P. *Angew. Chem., Int. Ed.* **2006**, *45*, 3501–3503.
(11) Balde, C. P.; Hereijgers, B. P. C.; Bitter, J. H.; de Jong, K. P. *J. Am. Chem. Soc.* **2008**, *130*, 6761–6765.
(12) Zheng, S. Y.; Fang, F.; Zhou, G. Y.; Chen, G. R.; Ouyang, L. Z.; Zhu, M.; Sun, D. L. *Chem. Mater.* **2008**, *20*, 3954–3958.
(13) Cliff, M.; Tepper, F.; Lisetsky, V. 37th AIAA/ASME/SAE/ASEE JPC Conference & Exhibit, Salt Lake City, UT, July 8—11, 2001; p 1.
(14) (a) Kwon, Y. S.; Gromov, A. A.; Ilyin, A. P. *Combust. Flame* **2002**, *131*, 349–352. (b) Kwon, Y. S.; Gromov, A. A.; Ilyin, A. P.; Rim, G. H. *Appl. Surf. Sci.* **2003**, *211*, 57–67. (c) Kwon, Y. S.; Gromov, A. A.; Strokova, J. I. *Appl. Surf. Sci.* **2007**, *253*, 5558–5564.
(15) Mary, B.; Dubois, C.; Carreau, P. J.; Brousseau, P. *Rheol. Acta* **2006**, *45*, 561–573.
(16) (a) Guo, L. G.; Song, W. L.; Xie, C. S.; Zhang, X. T.; Hu, M. L. *Mater. Lett.* **2007**, *61*, 3211–3214. (b) Guo, L. G.; Song, W. L.; Hu, M. L.; Xie, C. S.; Chen, X. *Appl. Surf. Sci.* **2008**, *254*, 2413–2417.
(17) Haber, J. A.; Buhro, W. E. *J. Am. Chem. Soc.* **1998**, *120*, 10847–10855.
(18) Higa, K. T.; Johnson, C. E.; Hollins, R. A. U.S. Patent 5,885,321, 1999.
(19) Foley, T. J.; Johnson, C. E.; Higa, K. T. *Chem. Mater.* **2005**, *17*, 4086–4091.
(20) (a) Jouet, R. J.; Warren, A. D.; Rosenberg, D. M.; Bellitto, V. J.; Park, K.; Zachariah, M. R. *Chem. Mater.* **2005**, *17*, 2987–2996. (b) Jouet, R. J.; Carney, J. R.; Granholm, R. H.; Sandusky, H. W.; Warren, A. D. *Mater. Sci. Technol.* **2006**, *22*, 422–429.
(21) Eckert, J.; Holzer, J. C.; Ahn, C. C.; Fu, Z.; Johnson, W. L. *Nanostruct. Mater.* **1993**, *2*, 407–413.
(22) Pozarnsky, G. A. U.S. Patents 6,676,727 and 6,689,190, 2004.
(23) Shin, H. K.; Shin, H. J. U.S. Patent 6,399,772, 2002.
(24) Marlett, E. M.; Park, W. S. *J. Org. Chem.* **1990**, *55*, 2968–2969.
(25) Valiyaveettil, S.; Gans, C.; Klapper, M.; Gereke, R.; Mullen, K. *Polym. Bull.* **1995**, *34*, 13–19.
(26) Fedotova, T. D.; Glotov, O. G.; Zarko, V. E. *Propellants, Explos., Pyrotech.* **2000**, *25*, 325–332.
(27) Klug, H. P.; Alexander, L. E. *X-ray Diffraction Procedures*; John Wiley & Sons: New York, 1959.
(28) Sardar, S. A.; Duschek, R.; Blyth, R. I. R.; Netzer, F. P.; Ramsey, M. G. *Surf. Sci.* **2000**, *468*, 10–16.
(29) Crowell, J. E.; Chen, J. G.; Yates, J. T., Jr. *J. Chem. Phys.* **1986**, *85*, 3111–3122.
(30) Fisher, G. L.; Hooper, A. E.; Opila, R. L.; Allara, D. L.; Winograd, N. *J. Phys. Chem. B* **2000**, *104*, 3267–3273.
(31) Crowell, J. E.; Chen, J. G.; Yates, J. T., Jr. *J. Electron Spectrosc. Relat. Phenom.* **1986**, *39*, 97–106.
(32) Zhukov, V.; Popova, I.; Fomenko, V.; Yates, J. T., Jr. *Surf. Sci.* **1999**, *441*, 240–250.

AM800209M